Chapter 2
Circularly Polarized Luminescence of Axially Chiral Binaphthyl Fluorophores

Yoshitane Imai

Abstract Axially chiral fluorophores bearing a variety of functionalities have been successfully developed using chiral binaphthyl units. These axially chiral binaphthyl fluorophores emit circularly polarized luminescence (CPL) in their solution-dissolved states, organic polymer-film-dispersed states, and inorganic pellet-dispersed states. The CPL emitted from an axially chiral binaphthyl fluorophore is easily tuned by (1) adjusting the dihedral angle in the binaphthyl unit, (2) employing the neighboring group effect between binaphthyl units, and (3) controlling their external environments, without the need for the enantiomeric compound.

2.1 Introduction

Organic compounds with chiroptical properties are very important for the development of new functional organic materials.

Axially chiral binaphthyl is a significant fundamental chiral unit that is used to introduce chirality into molecules and materials. An axially chiral binaphthyl organic fluorophore that can emit circularly polarized luminescence (CPL) is therefore very useful, since the binaphthyl unit exhibits both chirality and fluorescence [1–20].

In this chapter, the solution- and solid-state CPL properties of various axially chiral binaphthyl fluorophores are introduced.

Y. Imai (✉)
Kindai University, Osaka, Japan
e-mail: y-imai@apch.kindai.ac.jp

T. Mori (ed.), *Circularly Polarized Luminescence of Isolated Small Organic Molecules*, https://doi.org/10.1007/978-981-15-2309-0_2

2.2 Controlling Circularly Polarized Luminescence (CPL) Through the Dihedral Angle of the Axially Chiral Binaphthyl [21]

In this section, we report the chiroptical properties of axially chiral binaphthyl compounds in relation to the dihedral angle in the binaphthyl unit. For this purpose, two almost identical binaphthyl derivatives with the same (*S*)-axial chirality, namely, (*S*)-2,2′-diethoxy-1,1′-binaphthyl [(*S*)-**1**], as an open-type binaphthyl, and (*S*)-2,2′-(1,4-butylenedioxy)-1,1′-binaphthyl [(*S*)-**2**], as a closed-type, were chosen (Fig. 2.1).

The solution-state circularly polarized luminescence (CPL) and unpolarized photoluminescence (PL) spectra of the open-type (*S*)-**1** and the closed-type (*S*)-**2** in chloroform ($CHCl_3$) are shown in Fig. 2.2. (*S*)-**1** and (*S*)-**2** exhibit similar PL in $CHCl_3$; PL maxima (λ_{PL}) for (*S*)-**1** and (*S*)-**2** were observed at 365 and 368 nm, respectively, and the absolute values of their PL quantum yields (Φ_Fs) were 19% and 25%, respectively. The Φ_F value of (*S*)-**2** is greater than that of (*S*)-**1** because the ro-vibrational modes of (*S*)-**2** are limited compared to those of (*S*)-**1**, and the binaphthyl unit of (*S*)-**2** is more planar than that of (*S*)-**1**.

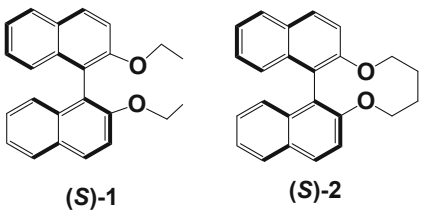

Fig. 2.1 Chiral binaphthyl fluorophores (*S*)-**1** and (*S*)-**2**

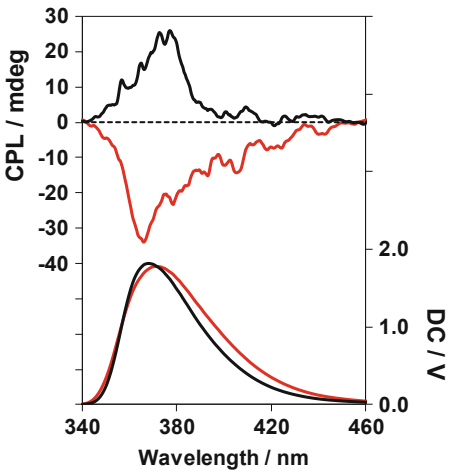

Fig. 2.2 CPL (upper) and PL (lower) spectra of (*S*)-**1** (black) and (*S*)-**2** (red) in $CHCl_3$ (1.0×10^{-3}M)

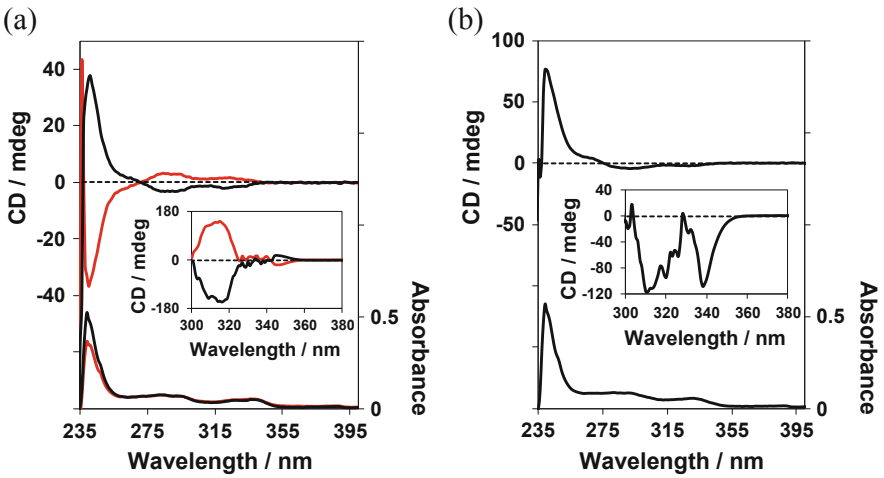

Fig. 2.3 CD (upper) and UV-Vis absorption (lower) spectra for (**a**) (*S*)-**1** (black) and (*R*)-**1** (red) and (**b**) (*S*)-**2** (black) in $CHCl_3$ (1.0×10^{-5} and 1.0×10^{-3}M (insets))

(*S*)-**1** and (*S*)-**2** emit CPL in $CHCl_3$. Surprisingly, although (*S*)-**1** and (*S*)-**2** have the same axial chirality, their CPL spectra show opposite signs; a positive (+) sign is observed for (*S*)-**1**, while (*S*)-**2** exhibits a negative (–) sign. To quantitatively compared the degrees of CPL and PL, we used the dimensionless Kuhn's anisotropy factor in the photoexcited state, which is defined as $g_{CPL} = 2(I_L - I_R)/(I_L + I_R)$, where I_L and I_R are the intensities of the left- and right-handed CPLs upon excitation with unpolarized light, respectively. The values of g_{CPL} were found to be about $+1.0 \times 10^{-3}$ for (*S*)-**1** and about -1.4×10^{-3} for (*S*)-**2**. These results suggest that the sign of the CPL depends on the nature of the binaphthyl ring (i.e., open or closed) in addition to axial chirality. To discuss the origin of the reversal in the sign of the CPL, solution-state circular dichroism (CD) and unpolarized UV-Vis absorption spectra for (*S*)-**1** and (*R*)-**1** were acquired, as shown in Fig. 2.3.

Several characteristic vibronic UV-Vis bands between 270 and 360 nm that arise from the ^1B_b transition moments of (*S*)-**1** and (*S*)-**2** were commonly observed. To quantitatively discuss the magnitude of the CD amplitude, we used the dimensionless Kuhn's anisotropy factor in the ground state, which is defined as $g_{CD} = \Delta\varepsilon/\varepsilon$. Values of g_{CD} for (*S*)-**1** and (*S*)-**2** at their first Cotton CD bands are about $+2.0 \times 10^{-4}$ (345 nm) and about -9.6×10^{-4} (338 nm), respectively. Evidently, the first Cotton CD band of (*S*)-**1** has opposite sign to that of (*S*)-**2**. This reversal in the CD sign, despite the same axial chirality, is possibly due to the difference in their chemical structures, i.e., whether the substituents are in the open or closed form. The opposite signs of the first Cotton CD bands are responsible for the opposite sign of the CPL bands observed for (*S*)-**1** and (*S*)-**2**.

To investigate the origins of the opposing CPL and CD spectral signs of (*S*)-**1** and (*S*)-**2**, CD spectra for (*S*)-**1** were determined computationally. Simulated

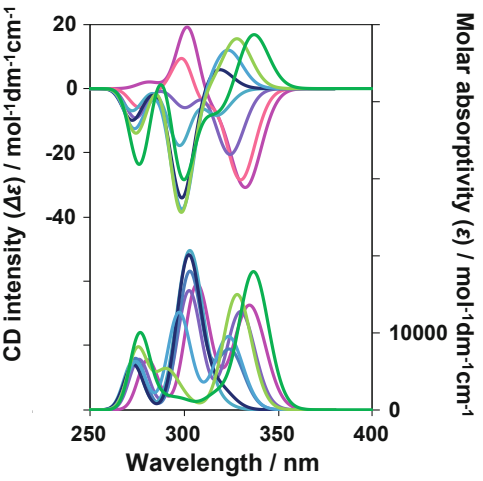

Fig. 2.4 CD and UV-Vis absorption spectra of (*S*)-**1** calculated as functions of the dihedral angle θ [+50° (—), +60° (—), +70° (—), +80° (—), +90° (—), +100° (—), +110° (—), +120° (—)] in the binaphthyl unit

dihedral-angle-dependent (θ = (O)C-C-C-C(O)) CD and UV-Vis absorption spectra of (*S*)-**1** are presented in Fig. 2.4. These simulations reveal that the sign of the first Cotton CD band of (*S*)-**1** is negative (−) for dihedral angles (θ) between about +50° and +85°, whereas the sign is positive (+) for θ between +85° and +120°.

These results suggest that the opposite first CD and CPL bands observed for (*S*)-**1** and (*S*)-**2** are attributable to differences in the θ values of the binaphthyl units in the ground and photoexcited states. In fact, the calculated equilibrium structures of (*S*)-**1** and (*S*)-**2** were observed to have θ values of +89.6° and +73.8° respectively, which suggests that the former has a positive first Cotton CD band (~340 nm) and the latter has a negative first Cotton CD band (~340 nm); these simulated results are consistent with experimental observations.

In conclusion, the CPL properties of an axially chiral binaphthyl fluorophore can be controlled by adjusting the dihedral angle of the binaphthyl unit in addition to its chirality. In general, the enantiomeric organic fluorophore is usually required to invert the sign of the CPL of a chiral fluorophore; however, the enantiomeric organic molecule is sometimes difficult to obtain. Therefore, controlling the sign of the CPL of axially chiral fluorophores through dihedral angle, without the need for the enantiomer, is a very useful technique.

2.3 Controlling the Sign of the Circularly Polarized Luminescence (CPL) from an Axially Chiral Binaphthyl Fluorophore by Solvent [22]

In Sect. 2.2, we reported that the sign of the CPL from a chiral binaphthyl fluorophore can be controlled by tuning the dihedral angle of the binaphthyl unit. In this section, solvent polarity control of the CPL sign of an axially chiral

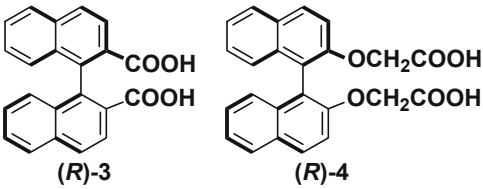

Fig. 2.5 Chiral binaphthyl fluorophores (*R*)-**3** and (*R*)-**4**

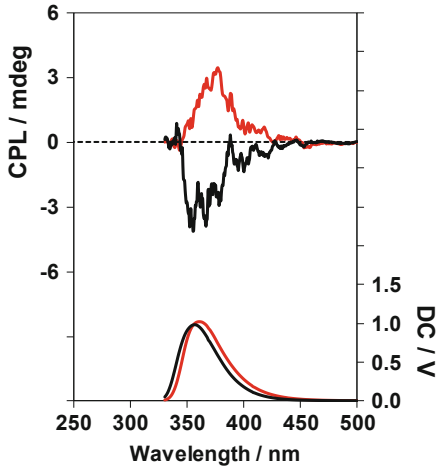

Fig. 2.6 CPL (upper) and PL (lower) spectra of (*R*)-**4** in $CHCl_3$ (black) and DMF (red) (1.0×10^{-4} M)

binaphthyl fluorophore in solution is demonstrated. As axially chiral binaphthyl fluorophore models, (*R*)-1,1′-binaphthyl-2,2′-dicarboxylic acid [(*R*)-**3**] and (*R*)-2,2′-(1,1′-binaphthyl-2,2′-diylbis(oxy))diacetic acid [(*R*)-**4**] were examined (Fig. 2.5).

The PL spectra of (*R*)-**3** and (*R*)-**4** were acquired in $CHCl_3$ and dimethylformamide (DMF) solutions, owing to their differing polarities. Dicarboxylic acid (*R*)-**3** did not exhibit PL in $CHCl_3$ and DMF solutions. On the other hand, (*R*)-**4** exhibited PL in both $CHCl_3$ and DMF, with PL maxima (λ_{PL}) observed at 356 and 361 nm, respectively, as shown in Fig. 2.6 (lower panel, black lines for $CHCl_3$ and red lines for DMF). The PL quantum yield (Φ_F) of (*R*)-**4** in $CHCl_3$ was found to be 25%. On the other hand, its Φ_F value increased to 39% in DMF, possibly due to the suppression of the rotational freedom of the binaphthyl unit as a result of hydrogen-bonding interactions with DMF. (*R*)-**4** exhibited a CPL signal in $CHCl_3$ and DMF, as shown in Fig. 2.6 (upper). Interestingly, although significant changes in λ_{em} were not observed in the two solvents, (*R*)-**4** exhibited opposite CPL signs in the two solvents: negative (−) in $CHCl_3$ and positive (+) in DMF. Their g_{CPL} values were found to be similar at about -0.18×10^{-3} for $CHCl_3$ and about $+0.19 \times 10^{-3}$ for DMF.

In order to elucidate the ground state chirality of **4**, CD and UV-Vis absorption spectra in $CHCl_3$ and DMF were acquired, as shown in Fig. 2.7a, b, respectively. The CD spectra of **4** exhibited significant differences in the first Cotton CD bands in

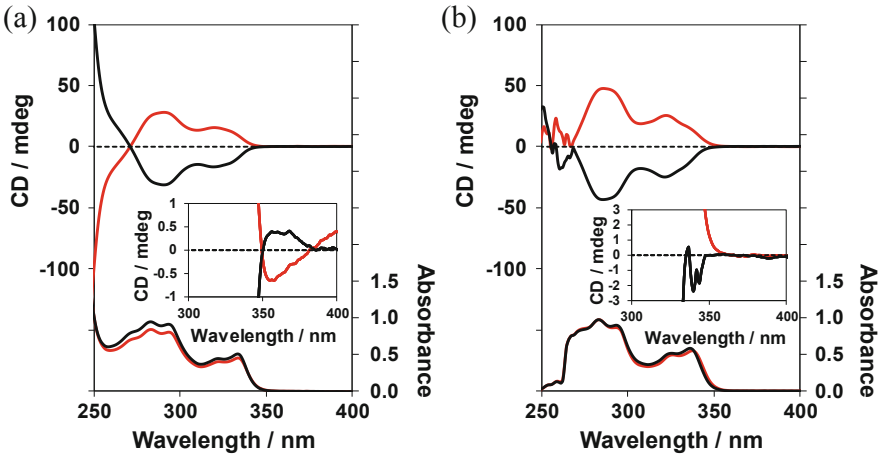

Fig. 2.7 CD (upper) and UV-Vis absorption (lower) spectra of (*R*)-**4** (red) and (*S*)-**4** (black) in (**a**) $CHCl_3$ and (**b**) DMF (1.0×10^{-4} and 1.0×10^{-3}M (insets))

$CHCl_3$ and DMF (Fig. 2.7; upper). The negative (−) sign ($\lambda_{CD} = 356$ nm) for (*R*)-**4** in $CHCl_3$ became positive (+) ($\lambda_{CD} = 337$ nm) in DMF. The g_{CD} value at the first Cotton CD band of (*R*)-**4** in $CHCl_3$ was about -0.33×10^{-3}, while a value of about $+0.38 \times 10^{-4}$ was observed in DMF.

The observed reversals of CPL and CD signs are possibly ascribable changes in the dihedral angles of the binaphthyl units. In DMF, the dihedral angle in the binaphthyl unit is smaller since the carboxylic acid groups in **4** interact efficiently with DMF molecules. Dipole-dipole and/or hydrogen-bonding interactions between DMF and the carboxylic acid groups on the binaphthyl units may also be responsible for the observed CD and CPL inversions in the ground and photoexcited states.

In conclusion, an axially chiral binaphthyl fluorophore can selectively emit positive or negative CPL through control of solvent type.

2.4 Controlling Circularly Polarized Luminescence (CPL) Through Neighboring Group Effects Involving Binaphthyl Units [23]

In Sect. 2.2, the signs of the CPL from chiral binaphthyl fluorophores were shown to be controllable by tuning the dihedral angle of the binaphthyl unit. As a more facile method for controlling the sign of the CPL from a chiral binaphthyl moiety while maintaining the same axial chirality, CPL sign control through neighboring-group effects between binaphthyl units has been reported. To enable this form of control, two binaphthyl derivatives with different numbers of chiral binaphthyl units that

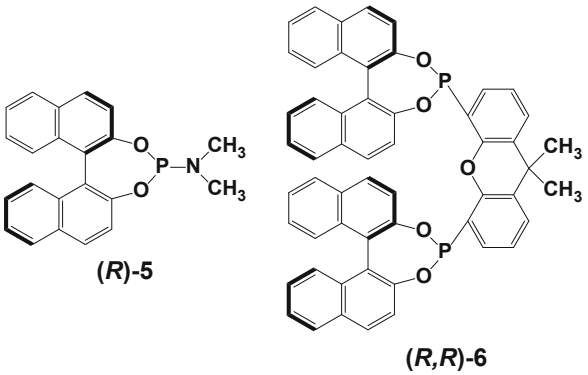

Fig. 2.8 Chiral binaphthyl fluorophores (*R*)-**5** and (*R*,*R*)-**6**

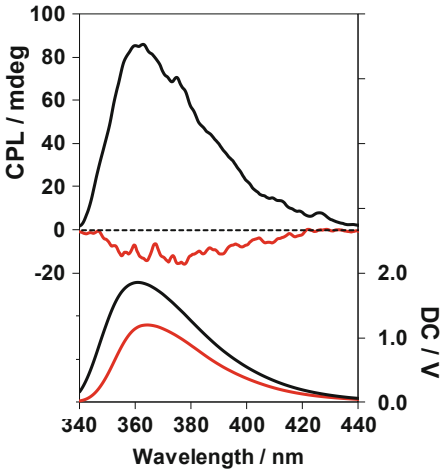

Fig. 2.9 CPL (upper) and PL (lower) spectra of (*R*)-**5** (black) and (*R*,*R*)-**6** (red) in $CHCl_3$ (1.0×10^{-3}M)

have the same (*R*)-axial chirality were investigated, namely, (*R*)-(−)-(3,5-dioxa-4-phosphacyclohepta[2,1-a:3,4-a′]dinaphthalen-4-yl)dimethylamine [(*R*)-**5**], with a single binaphthyl unit, and (11b*R*,11′b*R*)-4,4′-(9,9-dimethyl-9*H*-xanthene-4,5-diyl)-bis-di-naphtha[2,1-*d*:1′,2′-f][1,3,2]dioxaphosphepin [(*R*,*R*)-**6**], with two binaphthyl units (Fig. 2.8).

The CPL and PL properties of (*R*)-**5** and (*R*,*R*)-**6** were compared in $CHCl_3$. (*R*)-**5** and (*R*,*R*)-**6** exhibited PL maxima (λ_{PL}) at 361 and 362 nm in $CHCl_3$, respectively, as shown in Fig. 2.9. (*R*)-**5** and (*R*,*R*)-**6** emitted CPL in $CHCl_3$. Surprisingly, although (*R*)-**5** and (*R*,*R*)-**6** contain the same axially chiral binaphthyl unit, they exhibited oppositely signed CPL spectra, with a positive (+) sign observed for (*R*)-**5** and a negative (−) sign observed for (*R*,*R*)-**6**. The values of g_{CPL} were determined to be about $+3.4 \times 10^{-3}$ for (*R*)-**5** and -1.3×10^{-3} for (*R*,*R*)-**6**, where the $|g_{CPL}|$ value of **6** is smaller than that of **5** by a factor of three.

The solution-state CD and UV-Vis absorption spectra of (*R*)-**5** and (*R*,*R*)-**6** were acquired (Fig. 2.10). Several characteristic UV-Vis bands arising from π-π*

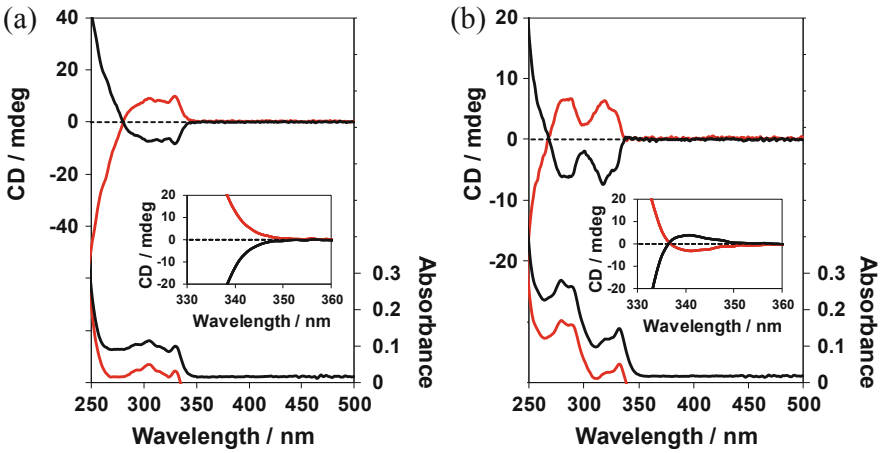

Fig. 2.10 CD (upper) and UV-Vis absorption (lower) spectra for (**a**) (*R*)-**5** (red) and (*S*)-**5** (black) and for (**b**) (*R*,*R*)-**6** (red) (*S*,*S*)-**6** (black) in $CHCl_3$ (1.0×10^{-5} and (insets) 1.0×10^{-4}M)

transitions involving the naphthyl groups in **5** and **6** were observed at approximately 270 and 360 nm, respectively. The signs of the CPL and the first Cotton CD band of (*R*)-**5** are both positive (+). Although the CD spectrum of (*R*,*R*)-**6** is similar to that of (*R*)-**5**, a weak negative (−) Cotton band was observed at the longest-wavelength edge in the spectrum of (*R*,*R*)-**6**. Because the CPL sign of (*R*,*R*)-**6** is negative (−), this weak negative (−) Cotton CD band may be responsible for the negative (−) sign of the CPL band. The $|g_{CD}|$ value at the first Cotton band ($\lambda_{CD} = 330$ nm) of **5** was determined to be about 4.2×10^{-3}; on the other hand, the $|g_{CD}|$ value of **6** at the first Cotton CD band ($\lambda_{CD} = 341$ nm) is about 2.5×10^{-4}, which is smaller than that of **5** by a factor of 17. Since the dihedral angles of the binaphthyl units in **5** and **6** are fixed, the opposite CD and CPL signs observed for (*R*)-**5** and (*R*,*R*)-**6**, despite having the same axial chirality, are due to the effects of the neighboring chiral binaphthyl units in (*R*,*R*)-**6**.

In conclusion, the CPLs of chiral binaphthyl fluorophores can be controlled by the number of neighboring chiral binaphthyl units, that is, by the effects of the neighboring binaphthyl units.

2.5 Dependence of the Circularly Polarized Luminescence (CPL) from Binaphthyl Units on External Environmental Factors [24]

In Sects. 2.2 and 2.4, the CPL signs of chiral binaphthyl luminophores with the same axial chirality were reported to be controllable by tuning the dihedral angle of the binaphthyl unit and by employing the neighboring group effect between fluorescent

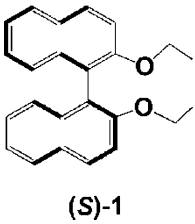

(*S*)-1

Fig. 2.11 Chiral binaphthyl fluorophore (*S*)-**1**

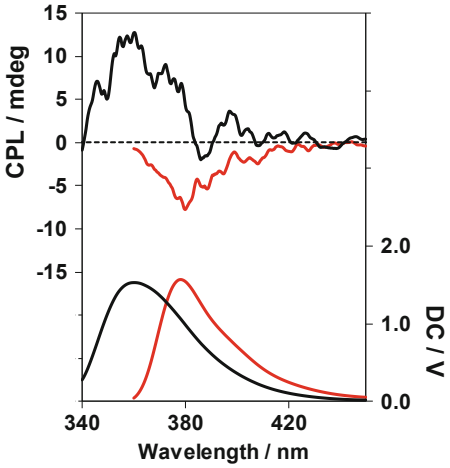

Fig. 2.12 CPL (upper) and PL (lower) spectra of (*S*)-**1** in PMMA film-dispersed (black) and KBr pellet-dispersed (red) states

binaphthyl units. In this section, an approach for the facile control of the CPL signs of chiral binaphthyl fluorophores involving the external solid-state environment is reported; (*S*)-2,2′-diethoxy-1,1′-binaphthyl [(*S*)-**1**] is used in this section as a model optically active binaphthyl fluorophore (Fig. 2.11). As the solid-state environment, organic poly(methyl methacrylate) (PMMA) and inorganic KBr are used.

The PL and CPL spectra of (*S*)-**1** in the PMMA film-dispersed state and the KBr pellet-dispersed state were acquired, as shown in Fig. 2.12. (*S*)-**1** dispersed in PMMA and KBr exhibited PL maxima (λ_{PL}) at 373 and 377 nm, respectively, with corresponding PL quantum yields (Φ_F) of 45% and 54%. Characteristically, the values of Φ_F for (*S*)-**1** were higher in the solid state than in $CHCl_3$ solution, which is possibly due to the suppression of vibrational deactivation of the molecule in the solid state.

(*S*)-**1** emits CPL both in the PMMA film-dispersed state and the KBr pellet-dispersed state. Surprisingly, (*S*)-**1** exhibited opposite CPL signs in these two states: positive (+) for the PMMA state and negative (−) for the KBr state. (*S*)-**1** has g_{CPL} values in the PMMA film and KBr pellet states of about $+7.9 \times 10^{-4}$ and -4.4×10^{-4}, respectively. The $|g_{CPL}|$ values of (*S*)-**1** in the PMMA and KBr states were slightly smaller than that of the $CHCl_3$ solution ($g_{CPL} = +1.0 \times 10^{-3}$).

The CD and UV-Vis absorption spectra of (*S*)-**1** in the PMMA film- and KBr pellet-dispersed states were also acquired (Fig. 2.13). Several UV-Vis bands were

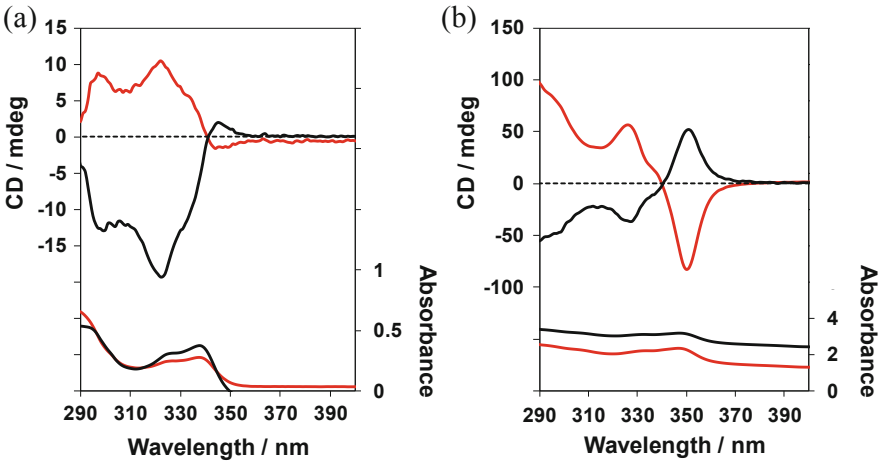

Fig. 2.13 CD (upper) and UV-Vis absorption (lower) spectra for (*S*)-**1** (black) and (*R*)-**1** (red) in (**a**) the PMMA film-dispersed state and (**b**) the KBr pellet-dispersed state

also observed at ~290 and ~380 nm in the solid state, which correspond to characteristic π-$\pi*$ transitions in the naphthyl groups of **1**. The CD spectra of (*S*)-**1** in two states are very similar in their long-wavelength tails. In contrast to the CPL spectra, the long-wavelength CD Cotton bands of (*S*)-**1** were both positive (+); the g_{CD} values of first Cotton CD band of (*S*)-**1** were $+3.5 \times 10^{-4}$ at $\lambda_{CD} = 345$ nm in the PMMA film-dispersed state and $+7.6 \times 10^{-4}$ at $\lambda_{CD} = 351$ nm in the KBr pellet-dispersed state. These g_{CD} values are slightly larger than that of the $CHCl_3$ solution of (*S*)-**1** ($g_{CD} = \sim+2.0 \times 10^{-4}$). The CD amplitudes of (*S*)-**1** in PMMA and KBr were evaluated as follows: $g_{CD} = ((\text{Abs}(L) - \text{Abs}(R))/|(\text{Abs}(L) + \text{Abs}(R))/2|$.

To determine the origins of the CPL and CD spectra of (*S*)-**1** in its PMMA-dispersed and KBr-dispersed states, the equilibrium structures of single molecules of **1** in solution (or PMMA) and KBr were compared. The equilibrium dihedral angle (θ = (O)C-C-C-C(O)) of (*S*)-**1** in $CHCl_3$ solution was determined to be 89.6°, while the structure of a single (*S*)-**1** molecule in the PMMA film-dispersed state was identical to that in solution. X-ray crystallography revealed that the dihedral angle θ of (*S*)-**1** in the solid state is 117.1°. Although these angles in the two states differ, the signs of the first Cotton CD bands of **1** in each state should be the same based on the simulated CD spectra reported in Sect. 2.2. These results suggest that the inversion of the CPL bands observed for **1** is determined by whether or not there are intermolecular neighboring group effects operating between chiral binaphthyl units in the photoexcited states.

In conclusion, the solid-state CPL of an axially chiral binaphthyl fluorophore can be controlled by changing its external solid-state matrix environment, from a PMMA film-dispersed state to a KBr pellet-dispersed state.

2.6 Dependence of Circularly Polarized Luminescence (CPL) on the Structure of the Tether Connecting Binaphthyl and Fluorescent Units [25]

The binaphthyl family contains one of the best chirality-inducing building blocks because binaphthyl units act as hinges that enable connections to a variety of molecular components, in addition to being a fluorescence source. In this section, control of the sign of the CPL of a chiral non-luminophoric binaphthyl-driven pyrene excimer system is demonstrated with the help of freely rotating alkyl ether tethers. Binaphthyl-pyrene **7** containing long oligoether tethers composed of ten single bonds, and binaphthyl-pyrene **8** with shorter (six single bonds) alkyl ether tethers were used (Fig. 2.14). In these systems, the binaphthyl moiety acts as a molecular hinge.

The PL spectra of (*R*)-**7** and (*R*)-**8** in $CHCl_3$ solutions are provided in the lower parts of Fig. 2.15. Both compounds exhibit almost identical PL maxima (λ_{PL}: 465 and 480 nm for (*R*)-**7** and 462 and 480 nm for (*R*)-**8**). Although these PL bands are intense, the monomeric PL bands at ~380 nm are very weak. This feature is ascribable to intramolecularly sterically constrained dimeric pyrenes in their S_0 states.

In contrast to their PLs, (*R*)-**7** and (*R*)-**8** exhibit opposite CPL signs in their S_1-state chiralities; they have the same binaphthyl (*R*)-chiralities as the S_1 state chirality: a negative (−) sign for (*R*)-**7** and a positive (+) sign for (*R*)-**8**. The excimeric origin of the CPLs of (*R*)-**7** and (*R*)-**8** in $CHCl_3$ are attributable to long-distance intramolecular chiral interactions between the two remote pyrenes attached to the chiral binaphthyl backbones through reorganization of the two photoexcited pyrenes in (*R*)-**7** and (*R*)-**8**. The g_{CPL} values of (*R*)-**8** ($+1.2 \times 10^{-3}$ at 462 nm and $+1.0 \times 10^{-3}$ at 480 nm) are larger than those of (*R*)-**7** (-0.41×10^{-3} at 465 nm and -0.46×10^{-3} at 480 nm). In this case, not only is the axial chirality of the binaphthyl in the S_0 state a critical factor that determines the CPL sign of the S_1 state, but so is the structure of the tether.

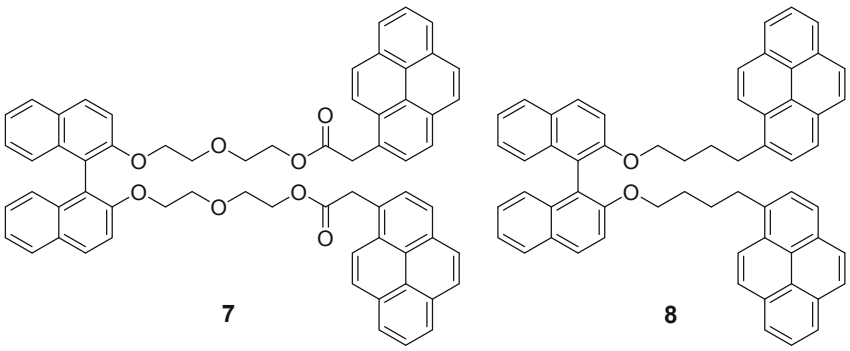

Fig. 2.14 Chiral binaphthyl-pyrene fluorophores **7** and **8**

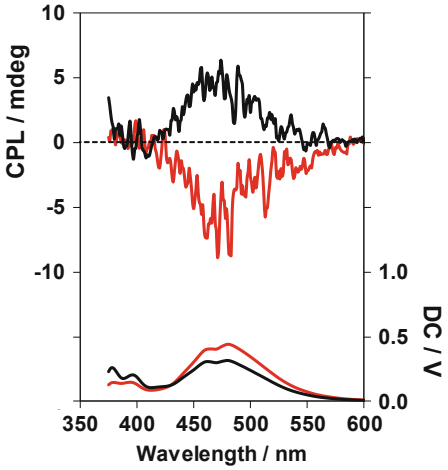

Fig. 2.15 CPL (upper) and PL (lower) spectra of (*R*)-**7** (red) and (*R*)-**8** (black) in $CHCl_3$ (1.0×10^{-5}M)

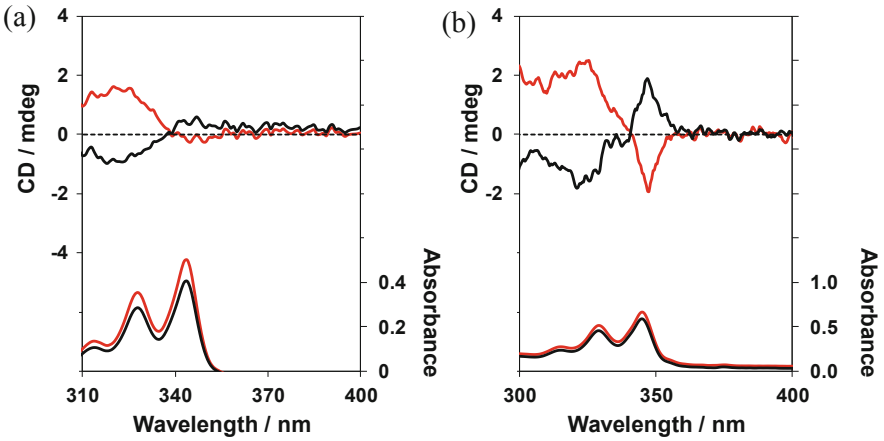

Fig. 2.16 CD (upper) and UV-Vis absorption (lower) spectra of (**a**) (*R*)-**7** (red) and (*S*)-**7** (black lies) and (**b**) (*R*)-**8** (red) and (*S*)-**8** (black) in $CHCl_3$ (1.0×10^{-5}M)

CD and UV-Vis absorption spectra of (*R*)-**7** [or (*S*)-**7**] and (*R*)-**8** [or (*S*)-**8**] in $CHCl_3$ were acquired (Fig. 2.16a, b, respectively). Several π-$\pi*$ vibronic UV transitions in the 315–355 nm range, which are characteristic of the pyrene and binaphthyl moieties, are clearly observed. The three well-resolved vibronic UV bands of (*R*)-**7** and (*R*)-**8**, which correspond to 0-0′ (~345 nm), 0-1′ (~329 nm), 0-2′ (~315 nm) bands, are observed; these three vibronic bands originate from the allowed ^1L_a transitions of the pyrene moieties in (*R*)-**7** and (*R*)-**8**.

The UV-Vis absorption spectra of (*R*)-**7** and (*R*)-**8** are almost identical and their CD spectra are also similar. The g_{CD} values of the 0-0′ band of (*R*)-**7** (at 343 nm) and (*R*)-**8** (at 345 nm) are similar, at only -0.22×10^{-4} and -0.67×10^{-4}, respectively. Surprisingly, the CD signals at the 0-0′ band of (*R*)-**7** and (*R*)-**8** both exhibit negative

(−) Cotton signs (Fig. 2.16, upper), even though (*R*)-**7** and (*R*)-**8** display opposite CPL signs (Fig. 2.15, upper). Characteristically, these g_{CD} values are smaller than the corresponding g_{CPL} values.

In this system, intermolecular associations of (*R*)-**7** and (*R*)-**8** in the S_0 state are neglected. In addition, an odd-even effect involving the number of atoms in the tethers may be a crucial factor that defines the signs of the CD and CPL signals; however, both tethers in **7** and **8** have odd numbers of atoms. These results lead to the conclusion that, although the chirality-oriented conformations of the two pyrenes in **7** and **8** in the S_0 states are similar, their relative orientations in the S_1 states may be very different, possibly with opposite handedness, which causes opposite CPL signs to be observed for **7** and **8**.

In conclusion, in axially chiral binaphthyls that connect fluorescent units, the CPL signs, which are generated by the two photoexcited fluorophores, can be controlled through tethered structures involving the axially chiral binaphthyl.

2.7 Cryptochiral Circularly Polarized Luminophores Based on Axially Chiral Binaphthyls [26]

In this section, the novel functional binaphthyl fluorophores designed using the CPL-controlling concepts discussed in Sects. 2.2 and 2.6, involving the 5,5′,6,6′,7,7′,8,8′-octahydro-1,1′-bi-2-naphthyl fluorophore **9** connected to two pyrenes through flexible ester tethers, is reported (Fig. 2.17).

The PL and CPL spectra of (*R*)-**9** and (*S*)-**9** in $CHCl_3$ are shown in Fig. 2.18. (*R*)-**9** exhibits an intense excimer PL band at 468 nm (λ_{PL}) of pyrene origin. In addition, a weak monomeric PL band at 396 nm is observed, which is ascribable to the sterically constrained intramolecular dimeric pyrene moieties in their S_0 states. (*R*)-**9** and (*S*)-**9** emit CPL and exhibit positive (+) and negative (−) CPL signs in their S_1-state structures, respectively. The absolute value of g_{CPL} for (*R*)-**9** in $CHCl_3$ is $+2.5 \times 10^{-3}$ at 454 nm.

Fig. 2.17 Chiral binaphthyl-pyrene fluorophore **9**

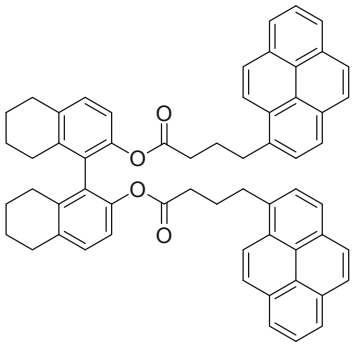

9

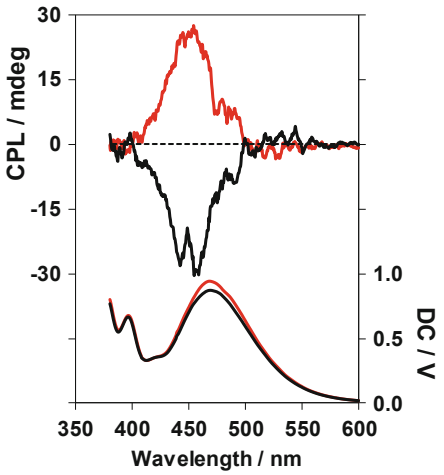

Fig. 2.18 CPL (upper) and PL (lower) spectra of (*R*)-**9** (red) and (*S*)-**9** (black) in $CHCl_3$ (1.0×10^{-5}M)

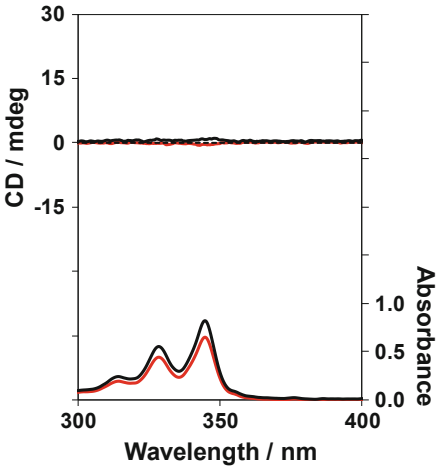

Fig. 2.19 CD (upper) and UV-Vis absorption (lower) spectra of (*R*)-**9** (red) and (*S*)-**9** (black) in $CHCl_3$ (1.0×10^{-5}M)

To evaluate the chiroptical properties of compounds **9** in their S_0-state structures, CD and UV-Vis absorption spectra of (*R*)-**9** and (*S*)-**9** were acquired (Fig. 2.19). The UV-Vis absorption spectra of (*R*)- and (*S*)-**9** exhibit three main π-$\pi*$ vibronic transitions (^1L_a transitions) between 315 and 360 nm that correspond to the pyrene moieties. Surprisingly, the intensities of the CD bands of (*R*)-**9** were noticeably weak, and no CD bands of (*R*)-**9** were detected in the 250–300 nm range, which suggests that, due to its pivotal framework, chiral molecular system **9** acts as a cryptochiral CPL fluorophore that has no detectable CD signals.

A mechanism for this cryptochirality has been hypothesized. The two pyrene units in **9** adopt an almost achiral T-shaped structure in the ground S_0 state, resulting in a θ value of about 80–90° in the axially chiral octahydrobinaphthyl unit, resulting in an almost undetectable CD spectrum. On the other hand, in the S_1 state, the two

pyrene units transform themselves into a chirally π-stacked arrangement. These changes in configuration are responsible for the cryptochiral behavior observed, namely, the ultra-weak CD and intense CPL bands of excimer origin that are due to the two floppy pyrene units that sandwich the octahydrobinaphthyl moiety.

In conclusion, a CD-silent/CPL-active cryptochiral binaphthyl fluorophore was successfully created by connecting an axially chiral binaphthyl and two fluorescent pyrene units through flexible tethers. This system can concurrently control two chiral points (binaphthyl and pyrene) in the photoexcited state.

2.8 Controlling Circularly Polarized Luminescence (CPL) of Binaphthyl-Pyrene Fluorophores Using Fluidic and Glassy Media [27]

In Sects. 2.3 and 2.5, the CPL signs of chiral binaphthyl fluorophores with the same axial chirality were reported to be controllable, both in solution and in the solid state, by manipulating their external environments. In this section, a non-classical approach for the dual control of the λ_{CPL} and the CPL sign of a chiral organic fluorophore, by varying the external environment, e.g., by choosing $CHCl_3$ solution as the fluidic medium and PMMA film as the glassy solid medium, is reported. To that end, chiral binaphthyl-pyrene fluorophore **7** with oligoether tethers was used again as the model system (Fig. 2.20).

Interestingly, although the $CHCl_3$ solution-state PL of (*R*)-**7** shows the typical excimeric emission of its pyrene units, the PL of (*R*)-**7** dispersed in PMMA film shows a λ_{PL} shifted to a significantly shorter wavelength ($\lambda_{PL} = 393$ nm), while its Φ_F value was higher, at 46%, due to the suppression of thermal vibrational deactivation (Fig. 2.21, lower).

As expected, (*R*)-**7** exhibited CPL signals in $CHCl_3$ and PMMA film (Fig. 2.21, upper panel). The CPL wavelength also changed, as was observed for PL. In addition, (*R*)-**7** exhibited CPL signs that depended on the fluidic and glassy states; it was negative (−) in $CHCl_3$ solution (Fig. 2.15) and positive (+) in the PMMA film.

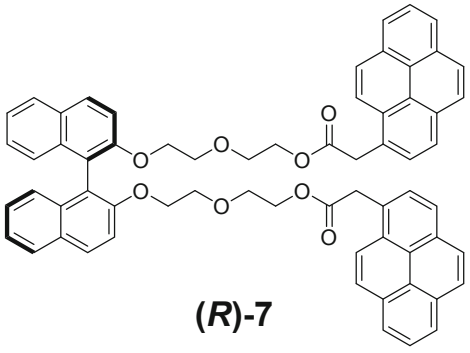

Fig. 2.20 Chiral binaphthyl-pyrene fluorophore (*R*)-**7**

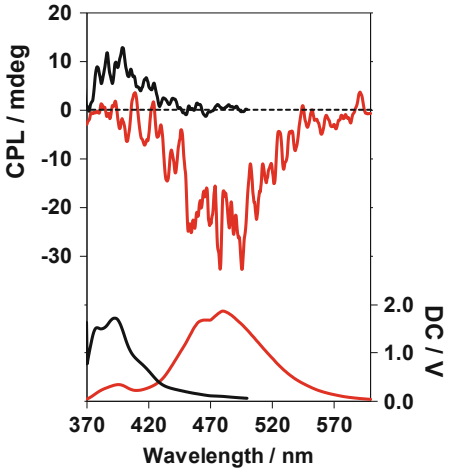

Fig. 2.21 CPL (upper) and PL (lower) spectra of (*R*)-**7** in $CHCl_3$ (1.0×10^{-3} M) (red) and in the PMMA film-dispersed state (black)

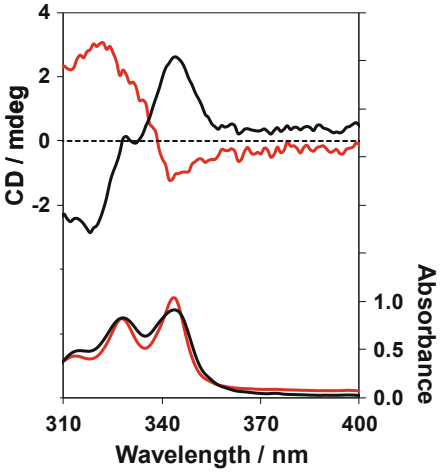

Fig. 2.22 CD (upper) and UV-Vis (lower) absorption spectra of (*R*)-**7** (red) and (*S*)-**7** (black) in the PMMA film-dispersed state

The g_{CPL} values were determined to be about -7.8×10^{-4} in $CHCl_3$ solution and about $+3.6 \times 10^{-4}$ in PMMA film. Hence, both λ_{CPL} and CPL sign of a chiral organic fluorophore are tunable by changing between fluidic $CHCl_3$ solution and a glassy PMMA film. On the other hand, the CD spectra of **7** in PMMA film (Fig. 2.22) are almost identical to those in $CHCl_3$ [Fig. 2.16a]; the g_{CD} value of the first Cotton CD band of (*R*)-**7** is about -3.8×10^{-5} at 344 nm in PMMA film (-5.9×10^{-5} in $CHCl_3$ solution).

In $CHCl_3$ solution, the two photoexcited pyrene moieties in (*R*)-**7** can approach each other more closely through reorganization. On the other hand, in PMMA film, although a remote intramolecular pyrene interaction produce chiral environment of pyrene units, the PMMA glassy solid inhibits the formation of a closer intramolecular pyrene excimer. The intramolecular reoriented mode involving the two pyrene

units is difficult to achieve upon photoexcitation; as a result, (*R*)-**7** exhibits monomer-like excimer CPL in PMMA film.

In conclusion, the CPL/PL characteristics of an axially chiral binaphthyl fluorophore connected to fluorescent units can be doubly controlled by selecting a fluidic $CHCl_3$ solution and a glassy PMMA film.

2.9 The Appearance of Circularly Polarized Luminescence (CPL) from a Chiral Binaphthyl-Terthiophene Fluorophore in the Solid State [28]

If chirality transfer from the chiral binaphthyl to a remote achiral fluorescent unit in a fluorescent binaphthyl system is not efficient in the solution state, CPL signals due to two remote fluorescent moieties may be not observed. In this section, the appearance of CPL from a dual-tandem fluorophoric molecular system, namely, (*R*)-**10** and (*S*)-**10** (Fig. 2.23), which consist of an axially chiral binaphthyl and two achiral terthiophenes, is reported. Terthiophene is a basic π-conjugated thiophene unit with superior fluorescence properties due to its long wavelength emission.

(*R*)-**10** exhibited the marked PL associated with terthiophene units in $CHCl_3$ solution, with a PL maximum (λ_{PL}) observed at 437 nm. Unfortunately, neither (*R*)- nor (*S*)-**10** exhibited any meaningful CPL spectrum in $CHCl_3$, presumably due to the highly flexible linkers between the terthiophenes and binaphthyl.

On the other hand, (*R*)-**10** exhibited marked PL with a λ_{PL} at 413 nm in the KBr solid state (Fig. 2.24, lower). Expectedly, (*R*)-**10** in KBr exhibited CPL with a g_{lum} value of about $+5.0 \times 10^{-4}$.

The solid-state CD and UV-Vis absorption spectra of (*R*)-**10** in the KBr pellet-dispersed state are shown in Fig. 2.25. Several π-$\pi*$ transitions associated with the terthiophene groups of **10**, in the 260–360 nm region are observed. The g_{CD} value at the Cotton CD band ($\lambda_{CD} = 342$ nm) of (*R*)-**10** is about -3.2×10^{-5}. The difference in the values of g_{CD} and g_{CPL} is possible ascribable to conformational changes in the ground and photoexcited states.

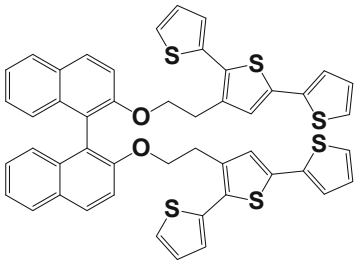

10

Fig. 2.23 Chiral binaphthyl-terthiophene fluorophore **10**

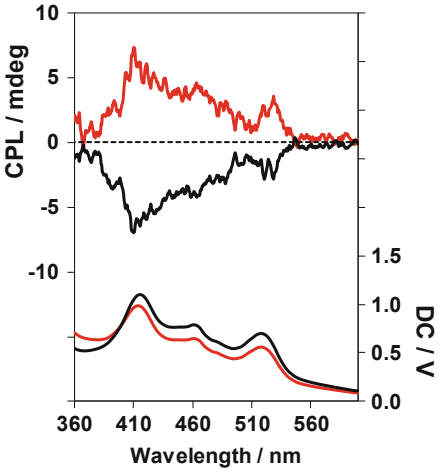

Fig. 2.24 CPL (upper panel) and PL (lower panel) spectra of (*R*)-**10** (red) and (*S*)-**10** (black) in the KBr pellet-dispersed state

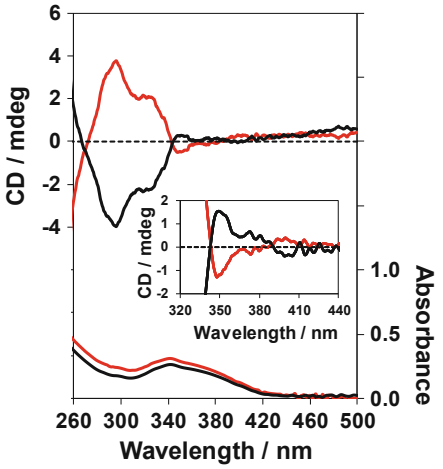

Fig. 2.25 CD (upper) and UV-Vis absorption (lower) spectra of (*R*)-**10** (red) and (*S*)-**10** (black) in the KBr pellet-dispersed state

Molecules densely packed in the solid state are surrounded by neighboring molecules. The appearance of solid-state CPL signals may be due to the following three factors: (1) efficient chirality transfer from the chirally rigid binaphthyl moiety to the terthiophene units in the solid state; (2) the very limited molecular motion in the solid state; and (3) efficient photoexcited-state chirality transfer from the binaphthyl when excited at 297 nm to certain chirally arranged terthiophene units.

In conclusion, unlike in the solution state, solid-state CPL is emitted from axially chiral binaphthyl fluorophores bearing remote fluorescent units aided by effective chirality transfer from the axially chiral binaphthyl moiety to the tethered fluorescent units.

2.10 Conclusion

Axially chiral binaphthyl is one of the most significant fundamental sources of chirality and fluorescence. An axially chiral binaphthyl fluorophore can emit circularly polarized luminescence (CPL) in the solution-dissolved state, PMMA film-dispersed state, and KBr pellet-dispersed state. The CPL emitted from an axially chiral binaphthyl fluorophore can easily be tuned by (1) tuning the dihedral angle in the binaphthyl unit, (2) employing the neighboring group effect that operates between binaphthyl units, and (3) controlling its external environment, without the need for the enantiomer. This chapter provides novel ideas for the design of novel CPL materials in the solution and solid state.

References

1. Bian Z, He Y-B, Gao L-X (2003) Circular dichroism and circularly polarized photoluminescence spectra of a new chiral conjugated polymers based on 1,1′-binaphthyl structure. Gaodeng Xuexiao Huaxue Xuebao 24:559–561
2. Sundar MS, Talele HR, Mande HM, Bedekar AV, Tovar RC, Muller G (2014) Synthesis of enantiomerically pure helicene like bis-oxazines from atropisomeric 7,7'-dihydroxy BINOL: preliminary measurements of the circularly polarized luminescence. Tetrahedron Lett 55:1760–1764
3. Park J, Yu T, Inagaki T, Akagi K (2015) Helical network polymers exhibiting circularly polarized luminescence with thermal stability. Synthesis via photo-cross-link polymerizations of methacrylate derivatives in a chiral nematic liquid crystal. Macromolecules 48:1930–1940
4. Ye Q, Zhu D, Xu L, Lu X, Lu Q (2016) The fabrication of helical fibers with circularly polarized luminescence via ionic linkage of binaphthol and tetraphenylethylene derivatives. J Mater Chem C 4:1497–1503
5. Uchida Y, Hirose T, Nakashima T, Kawai T, Matsuda K (2016) Synthesis and photophysical properties of a 13,13′-bibenzo[b]perylenyl derivative as a π-extended 1,1′-binaphthyl analog. Org Lett 18:2118–2121
6. Hirata S, Vacha M (2016) Circularly polarized persistent room-temperature phosphorescence from metal-free chiral aromatics in air. J Phys Chem Lett 7:1539–1545
7. Shi L, Zhu L, Guo J, Zhang L, Shi Y, Zhang Y, Hou K, Zheng Y, Zhu Y, Lv J et al (2017) Self-assembly of chiral gold clusters into crystalline nanocubes of exceptional optical activity. Angew Chem Int Ed 56:15397–15401
8. Shintani R, Misawa N, Takano R, Nozaki K (2017) Rhodium-catalyzed synthesis and optical properties of silicon-bridged arylpyridines. Chem Eur J 23:2660–2665
9. Nishikawa H, Mochizuki D, Higuchi H, Okumura Y, Kikuchi H (2017) Reversible broad-spectrum control of selective reflections of chiral nematic phases by closed-/open-type axially chiral azo dopants. Chem Open 6:710–720
10. Koiso N, Kitagawa Y, Nakanishi T, Fushimi K, Hasegawa Y (2017) Eu(III) chiral coordination polymer with a structural transformation system. Inorg Chem 56:5741–5747
11. Aoki R, Toyoda R, Kogel JF, Sakamoto R, Kumar J, Kitagawa Y, Harano K, Kawai T, Nishihara H (2017) Bis(dipyrrinato)zinc(II) complex chiroptical wires: exfoliation into single strands and intensification of circularly polarized luminescence. J Am Chem Soc 139:16024–16027

12. Song J, Wang M, Zhou X, Xiang H (2018) Unusual circularly polarized and aggregation-induced near-infrared phosphorescence of helical platinum(II) complexes with tetradentate salen ligands. Chem Eur J 24:7128–7132
13. Nishigaki S, Murayama K, Shibata Y, Tanaka K (2018) Rhodium-mediated enantioselective synthesis of a benzopicene-based phospha[9]helicene: the structure-property relationship of triphenylene- and benzopicene-based carbo- and phosphahelicenes. Mater Chem Front 2:585–590
14. Fujiki M, Koe JR, Mori T, Kimura Y (2018) Questions of mirror symmetry at the photoexcited and ground states of non-rigid luminophores raised by circularly polarized luminescence and circular dichroism spectroscopy: part 1. Oligofluorenes, oligophenylenes, binaphthyls and fused aromatics. Molecules 23:2606/1–2606/36
15. Wang Y, Harada T, Phuong LQ, Kanemitsu Y, Nakano T (2018) Helix induction to polyfluorenes using circularly polarized light: chirality amplification, phase-selective induction, and anisotropic emission. Macromolecules 51:6865–6877
16. Liu D, Zhou Y, Zhang Y, Li H, Chen P, Sun W, Gao T, Yan P (2018) Chiral BINAPO-controlled diastereoselective self-assembly and circularly polarized luminescence in triple-stranded europium(III) podates. Inorg Chem 57:8332–8337
17. Zhang X, Zhang Y, Zhang H, Quan Y, Li Y, Cheng Y, Ye S (2019) High brightness circularly polarized organic light-emitting diodes based on nondoped aggregation-induced emission (AIE)-active chiral binaphthyl emitters. Org Lett 21:439–443
18. Deng W-T, Qu H, Huang Z-Y, Shi L, Tang Z, Cao X, Tao J (2019) Facile synthesis of homochiral compounds integrating circularly polarized luminescence and two-photon excited fluorescence. Chem Commun 55:2210–2213
19. Maeda C, Ogawa K, Sadanaga K, Takaishi K, Ema T (2019) Chiroptical and catalytic properties of doubly binaphthyl-strapped chiral porphyrins. Chem Commun 55:1064–1067
20. Sun Z-B, Liu J-K, Yuan D-F, Zhao Z-H, Zhu X-Z, Liu D-H, Peng Q, Zhao C-H (2019) 2,2′-Diamino-6,6′-diboryl-1,1′-binaphthyl: a versatile building block for temperature-dependent dual fluorescence and switchable circularly polarized luminescence. Angew Chem 58:4840–4846
21. Kimoto T, Tajima N, Fujiki M, Imai Y (2012) Control of circularly polarized luminescence by using open- and closed-type binaphthyl derivatives with the same axial chirality. Chem Asian J 7:2836–2841
22. Okazaki M, Mizusawa T, Nakabayashi K, Yamashita M, Tajima N, Harada T, Fujiki M, Imai Y (2016) Solvent-controlled sign inversion of circularly polarized luminescent binaphthylacetic acid derivative. J Photochem Photobiol A 331:115–119
23. Amako T, Kimoto T, Tajima N, Fujiki M, Imai Y (2013) Dependence of circularly polarized luminescence due to the neighboring effects of binaphthyl units with the same axial chirality. RSC Adv 3:6939–6944
24. Kimoto T, Amako T, Tajima N, Kuroda R, Fujiki M, Imai Y (2013) Control of solid-state circularly polarized luminescence of binaphthyl organic fluorophores through environmental changes. Asian J Org Chem 2:404–410
25. Nakabayashi K, Kitamura S, Suzuki N, Guo S, Fujiki M, Imai Y (2016) Non-classically controlled signs in a circularly polarised luminescent molecular puppet: The importance of the wire structure connecting binaphthyl and two pyrenes. Eur J Org Chem 2016:64–69
26. Hara N, Yanai M, Kaji D, Shizuma M, Tajima N, Fujiki M, Imai Y (2018) A pivotal biaryl rotamer bearing two floppy pyrenes that exhibits cryptochiral characteristics in the ground state. Chem Select 3:9970–9973
27. Nakabayashi K, Amako T, Tajima N, Fujiki M, Imai Y (2014) Nonclassical dual control of circularly polarized luminescence modes of binaphthyl–pyrene organic fluorophores in fluidic and glassy media. Chem Commun 50:13228–13230
28. Taniguchi N, Nakabayashi K, Harada T, Tajima N, Shizuma M, Fujiki M, Imai Y (2015) Circularly polarized luminescence of chiral binaphthyl with achiral terthiophene fluorophores. Chem Lett 44:598–600